J. Ocean Univ. China (Oceanic and Coastal Sea Research)
DOI 10.1007/s11802-017-3287-7
ISSN 1672-5182, 2017 16 (6): 933-944
http://www.ouc.edu.cn/xbywb/
E-mail:xbywb@ouc.edu.cn

Structure Analyses of the Explosive Extratropical Cyclone: A Case Study over the Northwestern Pacific in March 2007

WANG Shuai[1), 2)], FU Gang[1), *], and PANG Huaji[1), 3)]

1) *College of Oceanic and Atmospheric Sciences*, *Ocean University of China*, *Qingdao* 266100, *P. R. China*
2) *Department of Physics*, *Imperial College London*, *London* SW7 2AZ, *UK*
3) *Qingdao Meteorological Bureau*, *Qingdao* 266003, *P. R. China*

(Received August 18, 2016; revised October 31, 2016; accepted December 19, 2016)

Abstract The synoptic situation and mesoscale structure of an explosive extratropical cyclone over the Northwestern Pacific in March 2007 are investigated through weather station observations and data reanalysis. The cyclone is located beneath the poleward side of the exit of a 200 hPa jet, which is a strong divergent region aloft. At mid-level, the cyclone lies on the downstream side of a well-developed trough, where a strong ascending motion frequently occurs. Cross-section analyses with weather station data show that the cyclone has a warm and moist core. A 'nose' of the cold front, which is characterized by a low-level protruding structure in the equivalent potential temperature field, forms when the cyclone moves offshore. This 'nose' structure is hypothesized to have been caused by the heating effect of the Kuroshio Current. Two low-level jet streams are also identified on the western and eastern sides of the cold front. The western jet conveys cold and dry air at 800–900 hPa. The wind in the northern part is northeasterly, and the wind in the southern part is northwesterly. By contrast, the eastern jet carries warm and moist air into the cyclone system, ascending northward from 900 hPa to 600–700 hPa. The southern part is dominated by the southerly wind, and the wind in the northern part is southwesterly. The eastern and western jets significantly increase the air temperature and moisture contrast in the vicinity of the cold front. This increase could play an important role in improving the rapid cyclogenesis process.

Key words explosive extratropical cyclone; meteorological bomb; rapid cyclogenesis; mesoscale structure; northwestern Pacific

1 Introduction

An explosive extratropical cyclone, which is also referred to as a 'meteorological bomb' (Sanders and Gyakum, 1980), is an extratropical cyclonic weather system that develops rapidly and is characterized by heavy precipitation and severe winds. Böttger *et al.* (1975) were the first to specifically study the rapid intensification of extratropical cyclones. Sanders and Gyakum (1980) defined explosive cyclogenesis as a condition in which a normalized reduction rate of central sea level pressure is at least 1 hPa h^{-1} averaged within 24 h. With significant improvements in measurement techniques in the last few decades, mid-latitude weather systems can be measured frequently and accurately. Therefore, Yoshida and Asuma (2004) suggested a new definition for explosive cyclogenesis, which can be written as

$$DR\ (\mathrm{hPa\ h^{-1}}) = \left(\frac{P_{t-6} - P_{t+6}}{12}\right)\left(\frac{\sin 60^\circ}{\sin\left|\frac{\varphi_{t-6} + \varphi_{t+6}}{2}\right|}\right), \qquad (1)$$

where DR denotes the deepening rate, t denotes time, P denotes the central sea level pressure, and φ denotes the latitude of cyclone center. Eq. (1) shows a definition of explosive cyclogenesis that is similar to the conventional one given by Sanders and Gyakum (1980) but with a shorter time period, *i.e.*, 12 h.

Explosive extratropical cyclones are cold-season events and more frequently observed over the Northwestern Pacific and Northern Atlantic (Sanders and Gyakum, 1980, Gyakum *et al.*, 1989). Lim and Simmonds (2002) further showed that the northwestern Pacific should be the area where explosive cyclogenesis occurs most frequently in the world. Explosive extratropical cyclones are commonly generated over East Asia and then move to the open ocean. Certain atmospheric and oceanic characteristics can be found before or during rapid cyclogenesis, and some of them can promote the deepening process of cyclogenesis. Gyakum and Danielson (2000) showed that as early as 72 h prior to explosive cyclogenesis over East Asia, disturbances on a synoptic scale usually appear at a level of 500 hPa in Central Siberia. Rapid cyclogenesis frequently developed above the south entrance of the strong sea surface temperature gradient (Sinclair, 1997) and beneath the dynamic divergence region with the equatorward entrance and poleward exit of upper-level jets. More-

* Corresponding author. E-mail: fugang@ouc.edu.cn

over, in anomaly fields, an anticyclone over East China and a westward-shifted Aleutian Low occasionally triggers the onset of rapid cyclogenesis by advecting cold air to the Kuroshio region, thereby enhancing atmospheric baroclinicity (Gyakum and Danielson, 2000).

Although explosive cyclogenesis has been extensively studied since the 1980s, an explosive extratropical cyclone is still difficult to forecast accurately because the main mechanism of this phenomenon remains unclear. However, previous studies (*e.g.*, Uccellini and Kocin, 1987) found that several atmospheric processes on various scales interact to create explosive development. Such processes include latent heating on a sub-synoptic scale (Anthes *et al.*, 1982), tropopause folding and jet streams at the upper level (Bleck, 1974; Uccellini *et al.*, 1984; Uccellini, 1986; Hoskins *et al.*, 1985), and intrusion of high potential vorticity (PV) from the stratosphere to the troposphere (Bosart and Lin, 1984; Uccellini *et al.*, 1985; Zehnder and Keyser, 1991; Reader and Moore, 1995).

From March 3 to 6, 2007, a weak synoptic-scale cyclonic circulation formed in Southern China, moved northeastwards progressively, and underwent explosive cyclogenesis while moving over the Northwestern Pacific. As a result of rapid cyclogenesis, the most severe snowstorm since 1951 hit Northern China. The average depth of snow caused by the storm in Liaoning Province was more than 20 cm. Surprisingly, strong storm surges, which are usually generated by high winds in tropical cyclones, occurred in the coastal areas around the Yellow Sea. Given the considerable economic exposure in East China, this explosive extratropical cyclone caused 14.6 billion RMB in economic losses, which is comparable to damage caused by a landfalling tropical cyclone.

To improve the forecasting and understanding of such devastating weather systems, we use explosive extratropical cyclone as an example to conduct a case study. The main objectives of this study are to investigate the synoptic-scale feature when a rapid cyclogenesis takes place and to analyze the mesoscale structures of the cyclone through observations. Weather station observations are used to conduct cross-section analysis of the frontal structure, which is the highlight of this study. The following section introduces the data sources. A case overview, including the synoptic analysis, is given in Section 3. A detailed mesoscale structure of the cold front is described in Section 4. The main findings are summarized in Section 5.

2 Data

The National Centers for Environmental Prediction (NCEP) FiNaL (FNL, 1˚×1˚) operational global analysis dataset (http://rda.ucar.edu/datasets/ds083.2/) was employed to identify the trajectory of the cyclone center. The NCEP Climate Forecast System Reanalysis dataset (CFSR, 0.5˚×0.5˚, Saha *et al.*, 2010) was used to analyze the cyclone lifecycle and synoptic conditions. To produce cloud images, the Multi-functional Transport SATellite (MTSAT) infrared channel data provided by Kochi University of Japan was applied (http://weather.is.kochi-u.ac.jp/archive-e.html). One of the highlights of this study is the use of NCEP ADP Global Upper Air (http://rda.ucar.edu/datasets/ds351.0/) and Surface (http://rda.ucar.edu/datasets/ds461.0/) Observational Weather Data to analyze the mesoscale structure.

3 Synoptic Analyses

As shown in Fig.1, from 00 UTC to 18 UTC 3 March 2007, the cyclone was generated over the Hubei Province, China, and moved northeastwards. After 18 UTC 3, the system passed over the Yellow Sea and moved toward the Korea Peninsula. The cyclone arrived at the Japan Sea around 00 UTC 6. Generally speaking, the cyclone moved along the coastal regions of East Asia. Fig.2 shows the time series of central sea level pressure and deepening rate. At 00 TUC 3, the central pressure was 1009 hPa and decreased to 997 hPa at 06 UTC 4. In accordance with the change in the deepening rate, this condition is the first rapid cyclogenesis period. From 12 UTC 4, the cyclone started to develop rapidly again, and this condition corresponds to the second peak of the deepening rate around 18 UTC 4, as shown in Fig.2. The central sea level pressure reached 986 hPa at 12 UTC 4 and dissipated gradually afterwards. At the same time, the deepening rate became negative; this condition refers to a dissipation stage. On the basis of the moving track and intensity change, the lifecycle of this cyclone can be divided into three stages.

1) Initial stage (from 00 UTC to 18 UTC 3 March 2007): the cyclone center was located inland, and the central sea level pressure started to drop with a progressive increase in the deepening rate.

2) Developing stage (from 19 UTC 3 to 00 UTC 5 March 2007): the cyclone center moved into ocean and northeastwards along the coast of the East Asia featured with a dual-rapid-cyclogenesis process.

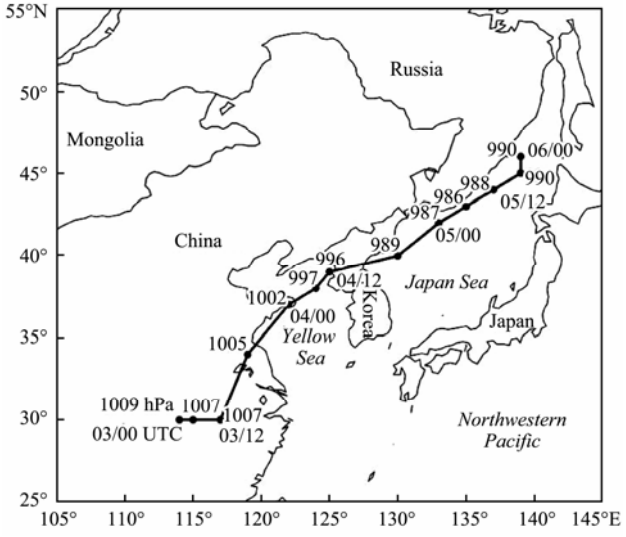

Fig.1 Trajectory of the cyclone center as determined from the FNL sea level pressure data from 00 UTC 3 to 00 UTC 6 March 2007.

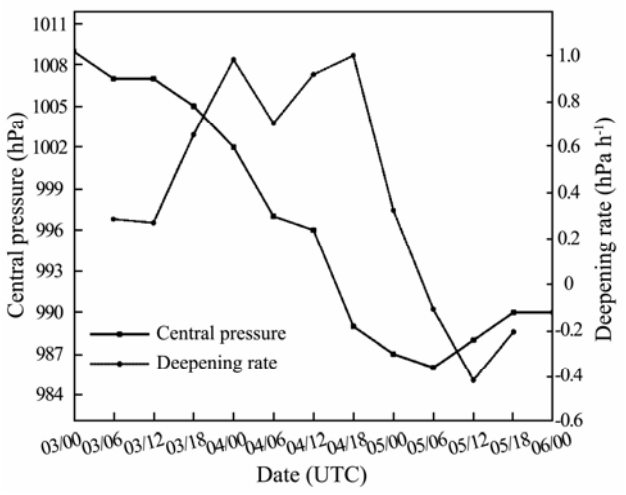

Fig.2 Time series of the central sea level pressure (solid line) and the deepening rate (dashed line).

3) Mature and decaying stage (from 01 UTC 5 to 00 UTC 6 March 2007): the cyclone center moved into the Japan Sea, and the deepening rate turned from positive to negative.

In the following analyses, we use 12 UTC 3, 12 UTC 4, and 12 UTC 5 to present the three stages defined above.

Fig.3 shows the synoptic conditions during the developing stage (12 UTC 4 March 2007) when the rapid cyclogenesis took place. Fig.3a shows that the cyclone is located beneath the downstream side of a 200 hPa trough. A jet stream establishes at a level of 200 hPa, and the cyclone is located on the poleward exit of the jet. Bluestein (1993) pointed out that this area is a strong divergence region, which corresponds to the strong divergence shown in Fig.3a; this condition is suitable for the development of a cyclonic system. At the 500 hPa level (Fig.3b), the surface cyclone center is located under the downstream side of a deep trough, which is consistent with the synoptic condition aloft. An ascending motion frequently takes under the downstream side of the trough at this level because of the strong divergence at 200 hPa. At this point, a typical extratropical cyclone structure can be identified at 850 hPa (Fig.3c). The considerable angle between the isotherm and isobaric contours indicates the significant baroclinicity that is essential for rapid extratropical cyclogenesis. As shown in Fig.3d, the diameter of the last closed isobar of the cyclone reaches approximately 1000 km at the sea surface, and most of East Asia was considerably influenced by the rapid cyclogenesis process at that time.

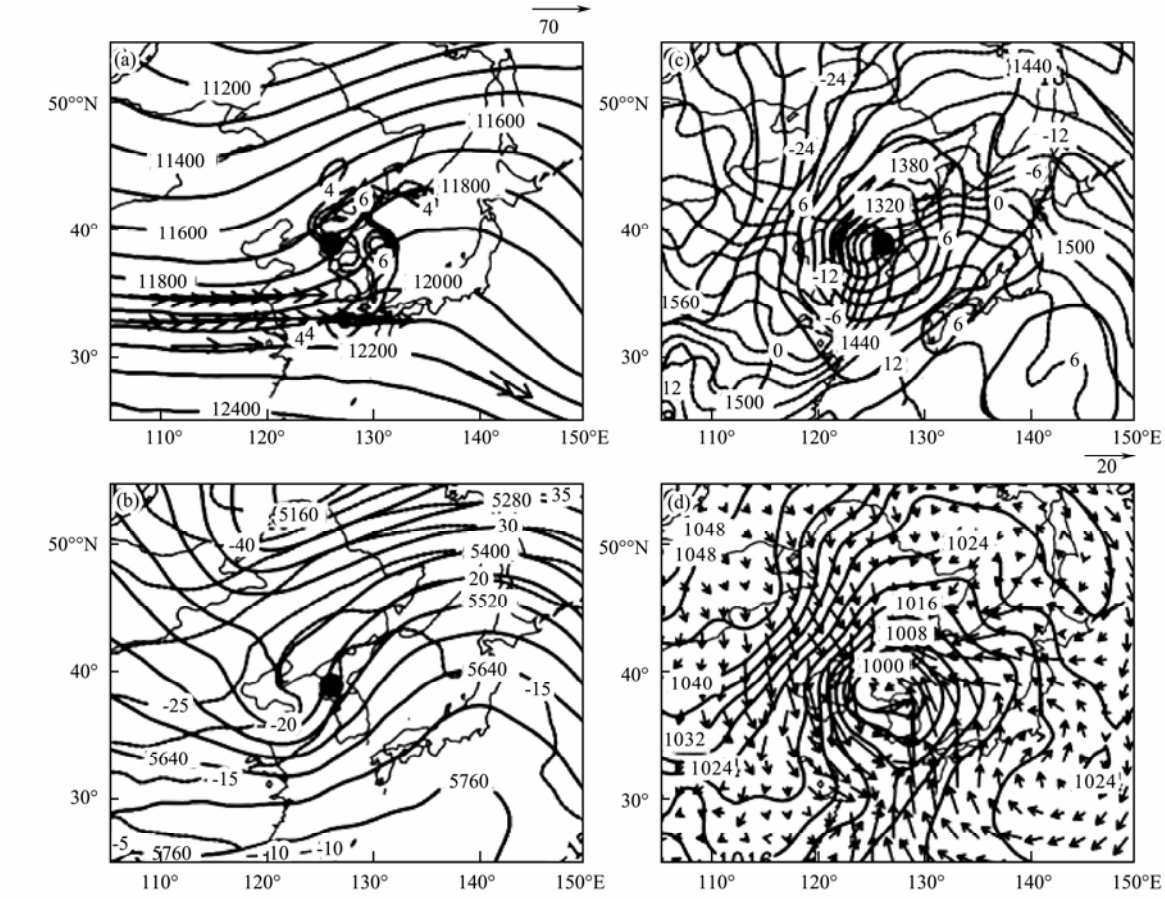

Fig.3 Weather maps at 12 UTC 4 March 2007. (a) 200 hPa geopotential height (solid line, gpm), horizontal divergence (dashed line, s^{-1}), and jet stream (arrow, only greater than 70 m s^{-1} shown). (b) 500 hPa geopotential height (solid line, gpm) and air temperature (dashed line, ℃). (c) 850 hPa geopotential height (solid line, gpm) and air temperature (dashed line, ℃). (d) Sea level pressure (solid line, hPa) and surface wind (arrow, m s^{-1}). The location of the surface cyclone center is denoted by the solid circle.

Fig.3c shows that the baroclinicity could be significant at the low level. To quantify the baroclinicity change during the development of the extratropical cyclone, the Eady growth rate maximum is calculated from 12 UTC 3 to 18 UTC 5 March 2007 (Fig.4). The Eady growth rate maximum (Hoskins and Valdes, 1990) is a widely used baroclinicity parameter, and it is defined as

$$\sigma_{\mathrm{BI}} = 0.31 \frac{f}{N} \left| \frac{\mathrm{d}\vec{V}}{\mathrm{d}z} \right|, \tag{2}$$

where σ_{BI} is the Eady growth rate maximum, f is the Coriolis parameter, N is the Brunt-Välsälä frequency, $\vec{V}$ is the horizontal wind vector, and z is the height of pressure levels. Fig.4 shows the baroclinicity parameter (σ_{BI}) change at 775 hPa, which is calculated within a 10° by 10° box in which the cyclone is centered. At 06 UTC 3 March, σ_{BI} is approximately 0.6 d^{-1}, which is the winter mean value in East Asia at approximately 780 hPa (Hoskins and Valdes, 1990). During the developing stage as it was previously defined, the mean σ_{BI} increases rapidly to approximately 1.3 d^{-1}, which is more than double relative to the winter mean value. The significant change of σ_{BI} indicates the occurrence of a stronge baroclinic energy conversion process that favors the explosive deepening of the extratropical cyclone (Iwao *et al.*, 2012).

As mentioned in the Introduction, the intrusion of high PV from the stratosphere to the troposphere could be important to the extratropical cyclone development. We next examine this top-to-bottom effect of PV at 12 UTC 4 March 2007. Fig.5a shows that the cyclone center is found below a high PV region at 200 hPa. The high PV aloft propogates downwards into the cyclone system, as shown by the cross-section analysis along line AB (Fig.5b). This downward intrustion of high PV favors cyclone development, as discussed by previous studies (Bosart and Lin, 1984; Uccellini *et al.*, 1985; Reader and Moore, 1995).

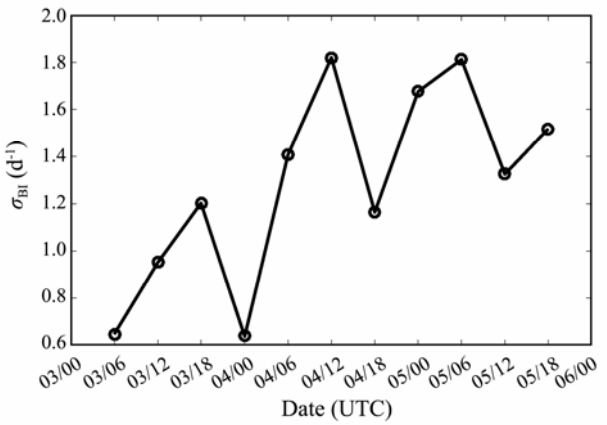

Fig.4 Time series of the Eady growth rate maximum (σ_{BI}, d^{-1}). σ_{BI} is calculated every 6 h within a 10° by 10° box in which the cyclone is centered.

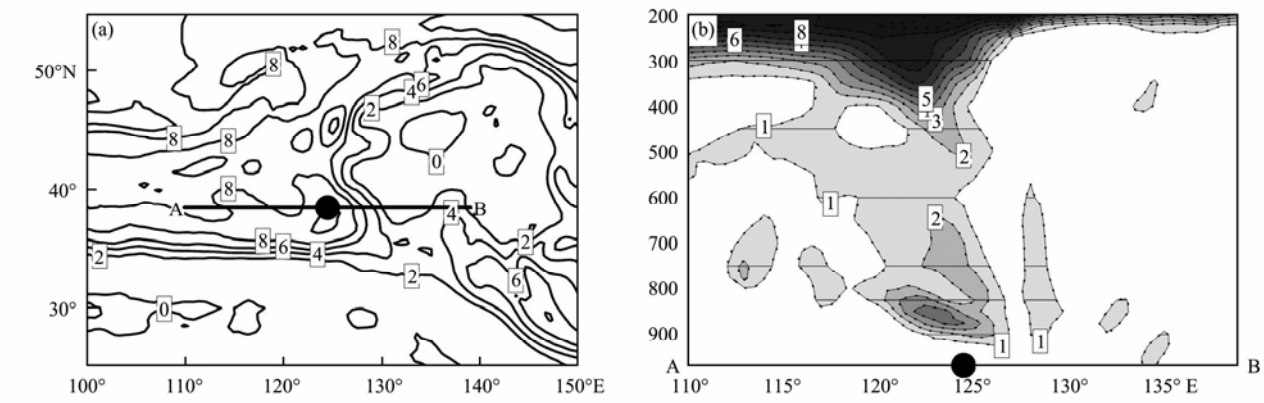

Fig.5 Potential vorticity with a unit of PVU ($10^{-6}\,\mathrm{K\,Pa^{-1}\,m\,s^{-1}}$) at 12 UTC 4 March 2007 (a) at the level of 200 hPa and (b) along the cross-section AB.

4 Mesoscale Features

4.1 Structure of the Cold Front

We next use weather station observations to analyze the mesoscale features of the frontal structure. The dense distribution of weather stations in the East Asia makes this type of analysis possible by connecting corresponding stations to form cross-sections. Cross-section lines CiDi (i=1, 2, 3, 4) and EiFi (i=1, 2, 3) are shown in Figs.6–10. The position of the surface front can be clearly detected by the wind bars. Cross-section CDs are designed to analyze the structure evolution during the period when cyclone moves offshore, as well as the structure of low-level jets. The first criterion for CD selection is to make the cross sections as perpendicular as possible to the cold front. The second criterion is that one of the cross sections should pass through the central area of the cyclone. The last criterion is to maintain approximately the same length for all the cross sections. Cross-section EFs are proposed to analyze the air temperature and humidity features of the cyclone. First, EFs are designed to be located along the cold front. Second, EFs should pass through the central part of the cyclone. Third, the length of EFs should be comparable. The zonal sections are selected at 12 UTC 4 and 5 March, whereas the EFs are

chosen at 00 UTC 4, 12 UTC 4, and 00 UTC 5.

Fig.6 shows that the front system moves from the land to the ocean at 12 UTC 4 March. As shown in Fig.11a, a cold front appears between 1000 km to 1500 km in C1D1. In Fig.11b, the cyclone center is located at 1600 km, and the central part of the cyclone features a cold front system. In C3D3 (Fig.11c), the slope of the front increases more significantly compared with the northern parts. To some extent, the front is essentially in the vertical direction with a small part that bumps to the east. A cold and dry air mass appears behind the front and remains there, as

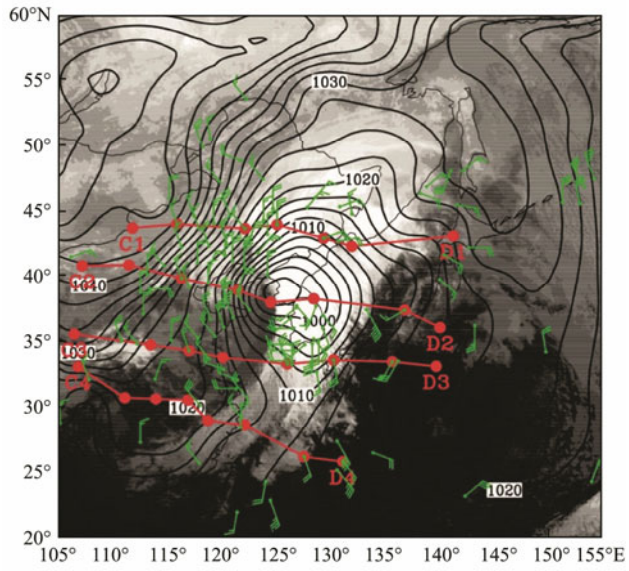

Fig.6 MTSAT satellite infrared image, surface wind (barb, m s^{-1}, a full barb is 4 m s^{-1}) at weather stations, and the sea level pressure (solid, hPa) at 12 UTC 4 March 2007. Lines CiDi (I=1, 2, 3, 4) are used for the zonal cross sections. The red dots along line C1D1 show the positions of sounding stations in Erenhot, Xilin, Tongliao, Changchun, Yanji, Vladivostok, and Sapporo. The red dots along line C2D2 show the positions of sounding stations in Linhe, Hohhot, Beijing, Dalian, Baengnyeongdo, Sokcho, Wajima, and Tateno. The red dots along line C3D3 show the positions of sounding stations in Pingliang, Zhengzhou, Xuzhou, Shenyang, Cheju, Fukuoka, Shionomisaki, and Hachijyojima. The red dots along line C4D4 show the positions of sounding stations in Hanzhong, Yichang, Wuhan, Anqing, Quxian, Hongjia, Naha, and Minamidaitojima.

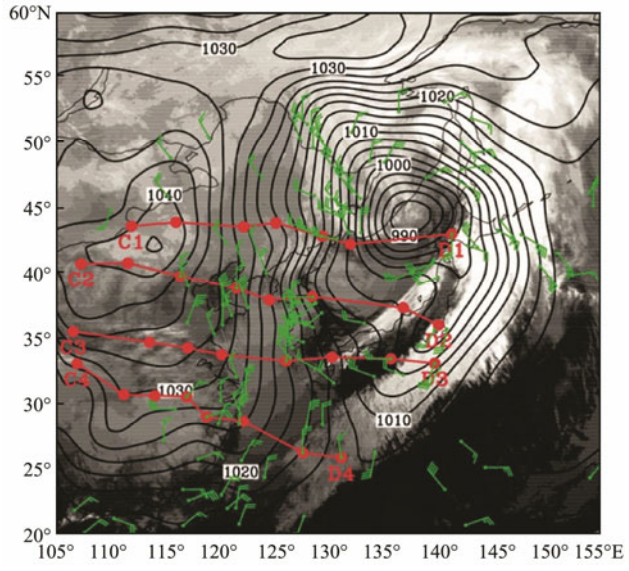

Fig.7 As in Fig.6, but for 12 UTC 5 March 2007.

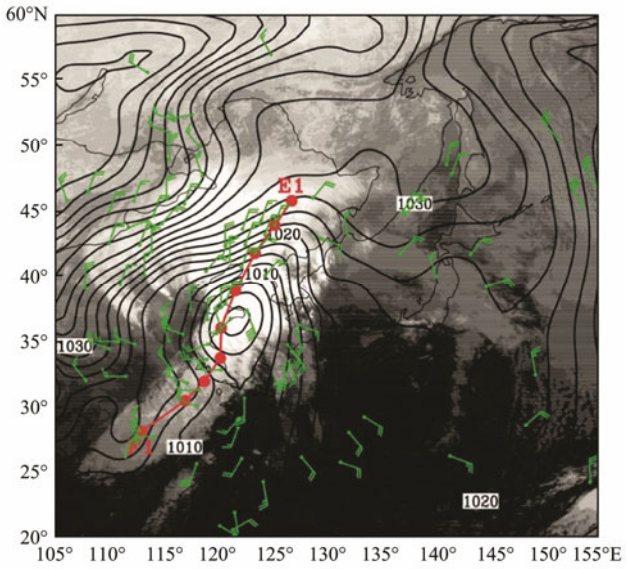

Fig.8 MTSAT satellite infrared image, surface wind (barb, m s^{-1}, a full barb is 4 m s^{-1}) at selected weather stations, and sea level pressure (solid line, hPa) at 00 UTC 4 March 2007. Line E1F1 is used for the meridional cross sections. The red dots along line E1F1 (from north to south) show the positions of sounding stations in Changchun, Shenyang, Dalian, Qingdao, Sheyang, Nanjing, Anqing, and Changsha.

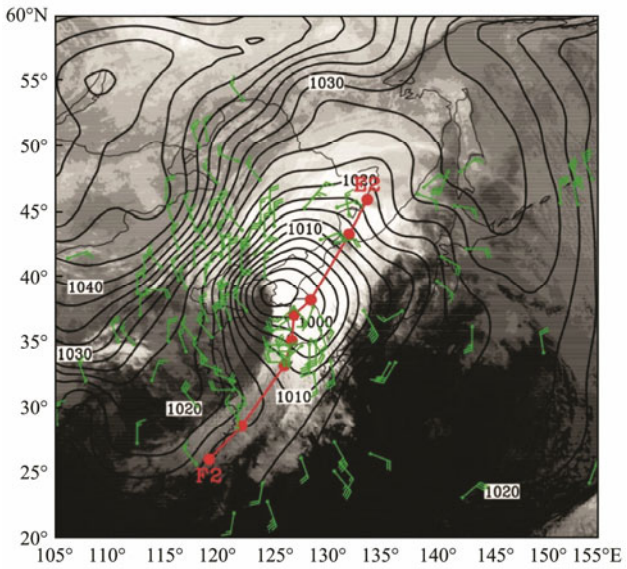

Fig.9 MTSAT satellite infrared image, surface wind (barb, m s^{-1}, a full barb is 4 m s^{-1}) at selected weather stations, and sea level pressure (solid line, hPa) at 12 UTC 4 March 2007. Line E2F2 is used for the meridional cross sections. The red dots along line E2F2 (from north to south) show the positions of sounding stations in Dalnerechensk, Vladivostok, Sokcho, Osan, Kwangju, Cheju, Hongjia, Fuzhou.

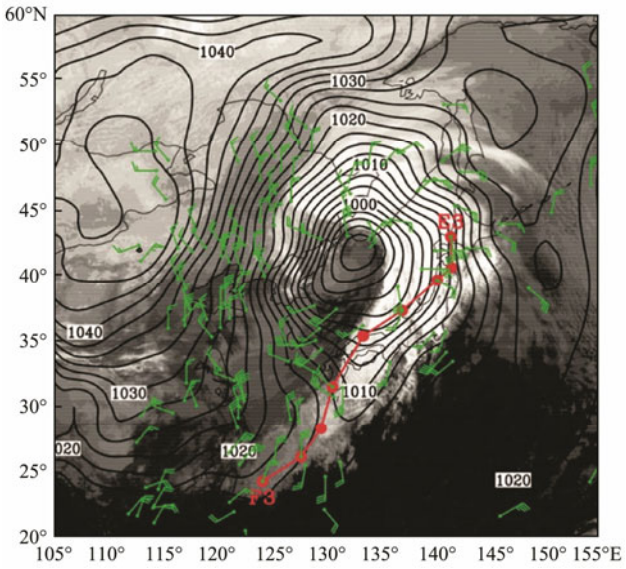

Fig.10 MTSAT satellite infrared image, surface wind (barb, $m\,s^{-1}$, a full barb is $4\,m\,s^{-1}$) at selected weather stations and sea level pressure (solid line, hPa) at 00 UTC 5 March 2007. Line E3F3 is used for the meridional cross sections. The red dots along line E3F3 (from north to south) show the positions of sounding stations in Misawa, Akita, Wajima, Yonago, Kagoshima, Naze, Naha, and Ishigakijima.

shown in Fig.11d.

Fig.12a (C1D1) shows that at 12 UTC 5, the central part of the cyclone is still controlled by the cold front system. The cold front in C2D2 is in the vertical direction, which is similar to the situation shown in C3D3 24 h prior (Fig.11c). A cold tongue extends to the east at 900 hPa and 1500 km. In C3D3 (Fig.12c), the eastward extension of the cold tongue is enhanced, which indicates a more intense intrusion of cold air. Fig.13 shows that at this time, the Kuroshio Current lies approximately 2500 km in C3D3. The existence of the warm current could slow down the air temperature drop near the sea surface due to the strong surface heat flux, as shown in Fig.13. The eastward movement of the cold front near the surface would therefore decelerate. The difference in the translation speed of the cold front in the vertical caused by the warm current results in a 'nose' structure of the cold front in the lower troposphere, as shown in Fig.12c at 2500 km and 850 hPa.

Cross-section EFs are employed to analyze the difference in the air temperature and humidity from north to south. Section E1F1 (Fig.14a) shows that the northern part of the cyclone is colder and drier than the southern part. A significantly warm and wet core can be observed from 800 hPa to 900 hPa. After 12 hours, E2F2 (Fig.14b)

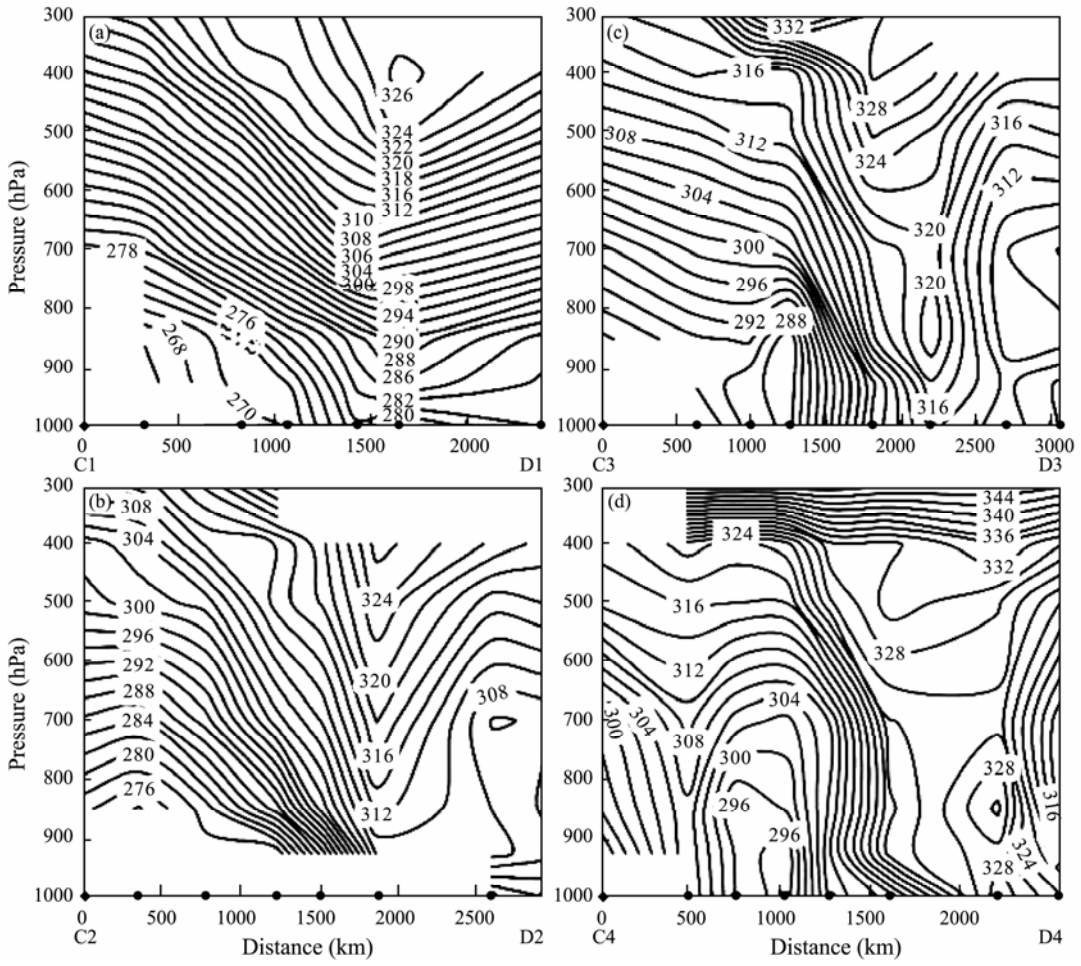

Fig.11 CiDi (I=1, 2, 3, 4) cross sections at 12 UTC 4 March 2007. Contours represent the equivalent potential temperature (K), and the dots denote the position of weather stations.

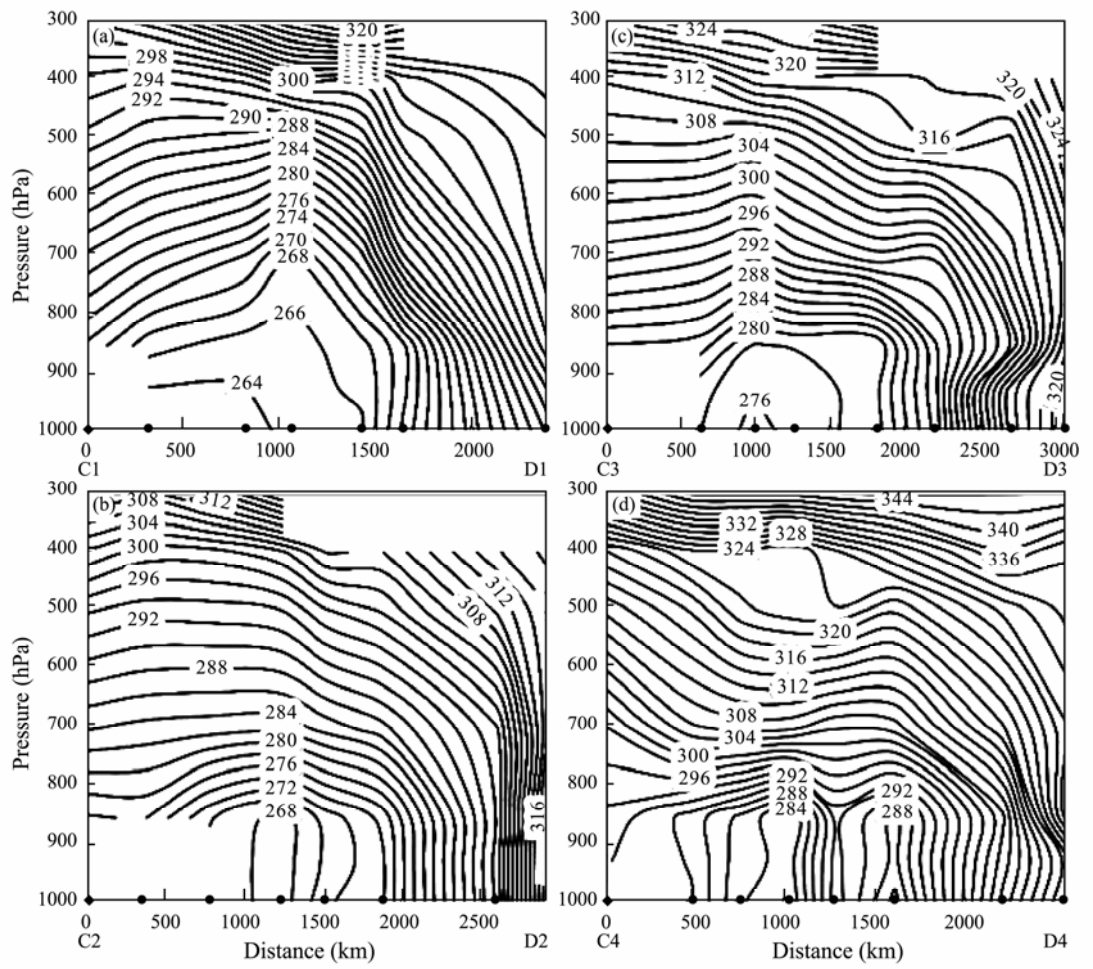

Fig.12 As in Fig.11, but for 12 UTC 5 March 2007.

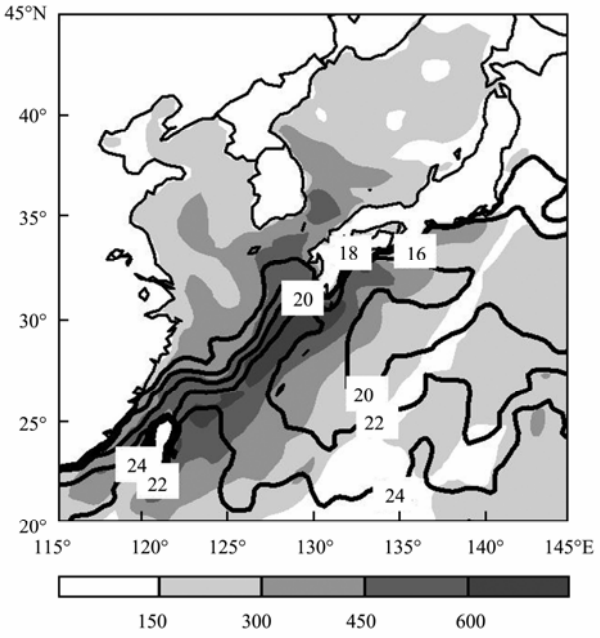

Fig.13 Sea surface temperature (black lines, ≥16℃ only) and surface heat flux (shaded, ≥150 W m^{-2} only) at 12 UTC 5 March 2007.

retains the basic features in the air temperature and humidity fields, but the wet and warm cores are separated. At 00 UTC 5 (Fig.14c), the warm core is more enhanced than it was 12 h prior. At this time, both cores descend and almost touch the underlying surface.

4.2 Low-Level Jets

We next focus on the developing stage (12 UTC 4 March) to analyze the low-level jets, which may play important roles in conveying warm/moist and cold/dry air into the cyclone system. In Fig.15 (12 UTC 4 March), C2D2, C3D3, and C4D4 go through the cold front, but C1D1 does not. In C1D1, two high-speed regions are observed; one is located at 850 hPa and 800 km, and the other is located at 600 hPa and 1500 km. The western jet descends to 900 hPa in C2D2 as the wind speed increases (30 m s^{-1}), whereas the eastern jet retains its height and strength. C3D3 shows that the low-level jet on the eastern side shifts to 925 hPa at 2200 km. At the same time, the western jet is difficult to identify. In C4D4 (Fig.15d), the western jet disappears completely, and the eastern jet also decays. Fig.12 shows that two low-level jet streams exist in the cyclone system, *i.e.*, a western jet and an eastern jet. A comparison with Fig.6 shows that, along the moving direction of the cold front, the western jet is located behind the cold front and the eastern one is in front of the cold front. In addition, the western jet basically remains the same height. By contrast, from south to north, the

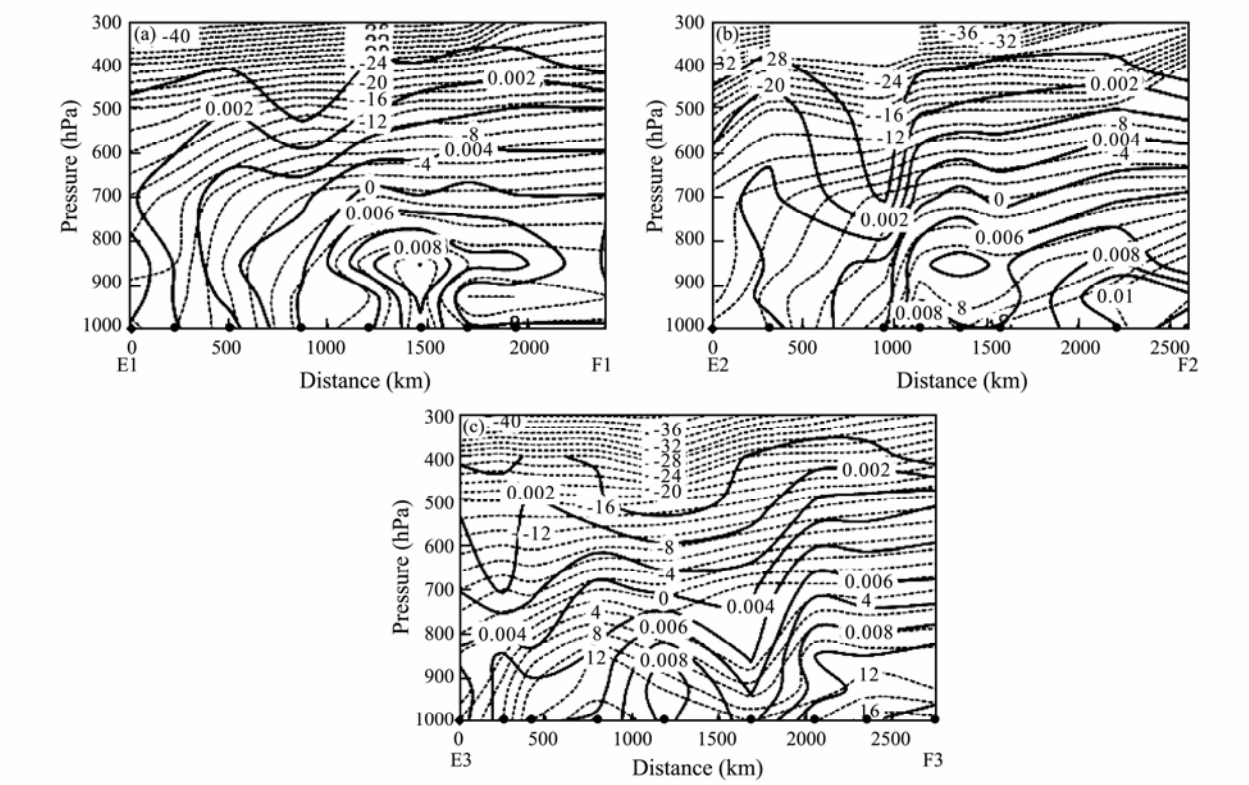

Fig.14 Vertical cross-section analyses along (a) E1F1 at 00 UTC 4, (b) E2F2 at 12 UTC 4, and (c) E3F3 at 00 UTC 5 March 2007. Solid lines show air temperature (℃), and dashed lines represent the specific humidity (kg kg^{-1}). Dots show the position of weather stations.

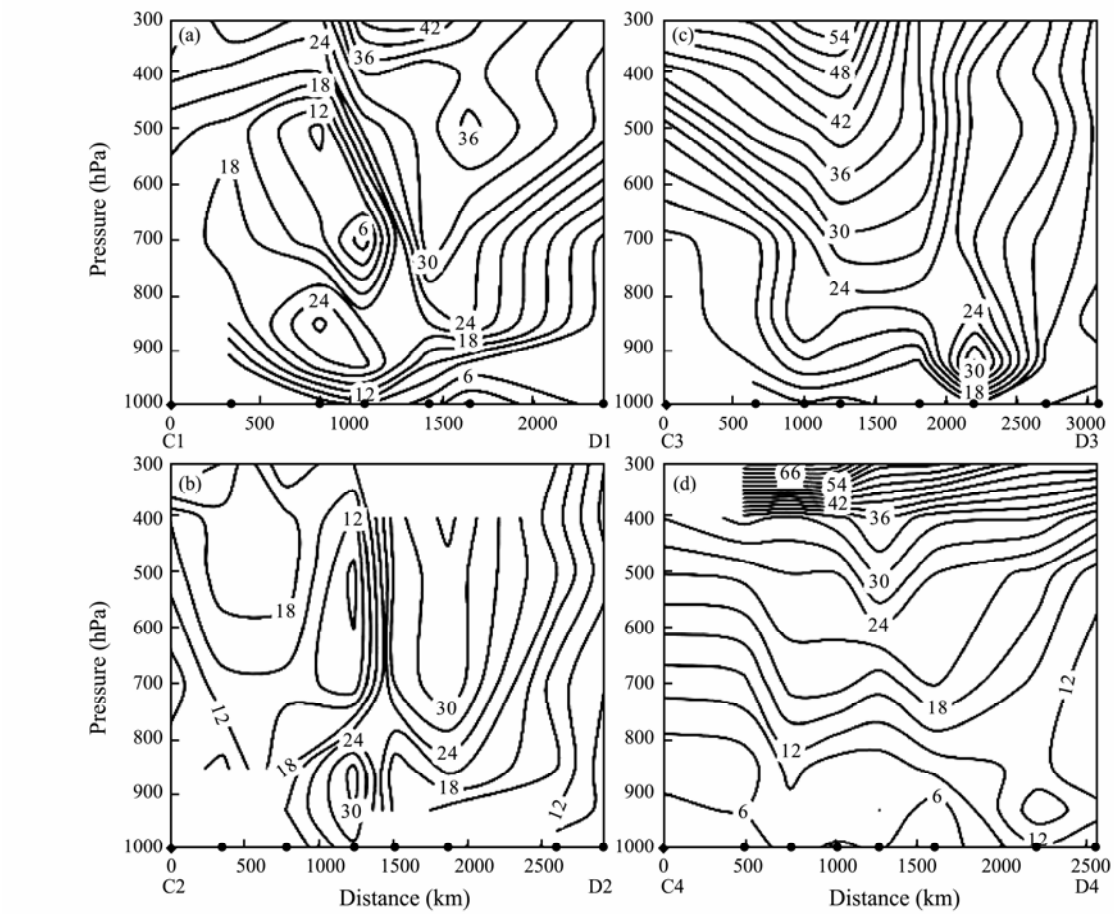

Fig.15 Vertical cross-section analyses along line CiDi (I=1, 2, 3, 4) at 12 UTC 4 March 2007. Contours represent the total horizontal wind speed (m s^{-1}). Dots show the positions of sounding stations.

eastern jet ascends significantly from 900 hPa to 600 hPa.

Two low-level jets have been identified; thus, we next focus on their directions. A comparison between Figs.16 and 15 shows that the western jet, which is behind the cold front, is dominated by the northerly wind, whereas the eastern jet, which is in front of the cold front, corresponds to the southerly wind. The magnitudes of the total wind and the meridional wind are comparable, thereby suggesting that these two low-level jets are mainly controlled by meridional flows. As a result of the opposing motions of the jets, strong cyclonic shear is generated in the vicinity of the cold front, as shown in Figs.16a, b, and c.

Even though these two low-level jets are dominated by meridional flows, we can still find some characteristics of these two jets in the zonal direction. For the western jet, from north to south (Figs.17a, b, and c), the zonal wind speed turns from negative to positive, which means that in the northern part, the western jet has a slightly easterly wind component but changes to the westerly wind in the southern part. As for the eastern jet, in the southern part (Figs.17d and c), the zonal component is almost zero, which, to some extent, refers to a purely meridional flow. However, the zonal component is changed to the westerly wind (Figs.17b and a) when the eastern jet ascends in the northern part.

Fig.18 shows the thermodynamic features of the eastern and western low-level jets. In C1D1 (Fig.18a), a warm and moist core appears at 700 hPa and 1500 km, which coincides with the location of the northern part of the eastern jet. On the western side of this warm and moist center, cold and dry tongues correspond to the eastern jet. The situations in C2D2 (Fig.18b) are similar to C1D1, apart from the lower altitude of the warm and moist center compared with its height shown in C1D1. The height change is consistent with the northward ascension of the eastern jet. The western jet becomes more concentrated as it shows a cold core for the first time as in C3D3.

On the basis of the above analyses, the basic features of the two low-level jets can now be summarized as follows:

Western jet: 1) The jet remains at the levels between 800 to 900 hPa; 2) the northern part (>36°N) is a northeasterly wind, whereas the southern part (<36°N) is a northwesterly wind; 3) the jet conveys the cold and dry air.

Eastern jet: 1) The jet ascends from 900 hPa in the south to 600–700 hPa in the north; 2) the southern part (<36°N) is dominated by the southerly wind and the northern part (>36°N) is a southwesterly wind; 3) the jet conveys the warm and moist air.

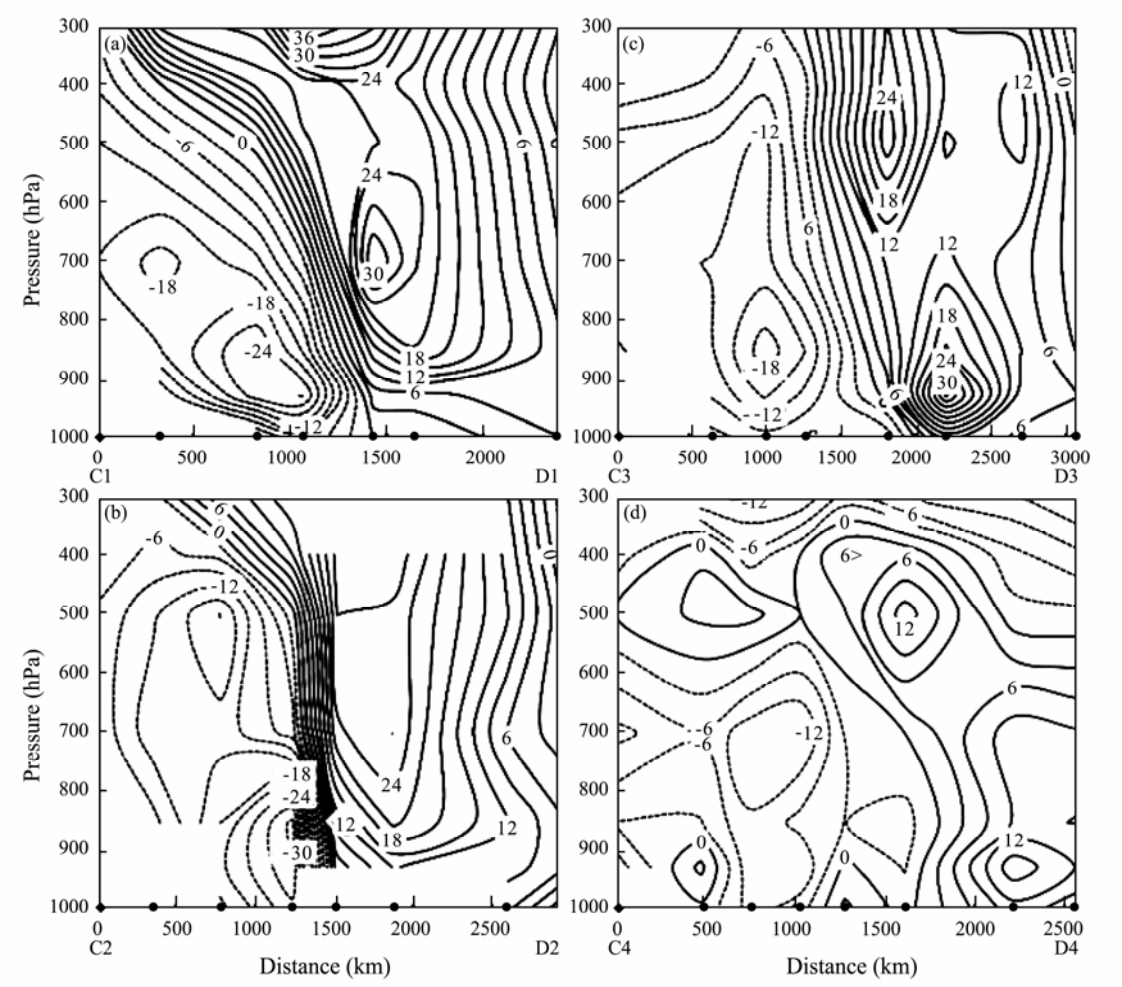

Fig.16 As in Fig.15, but for the meridional wind speed.

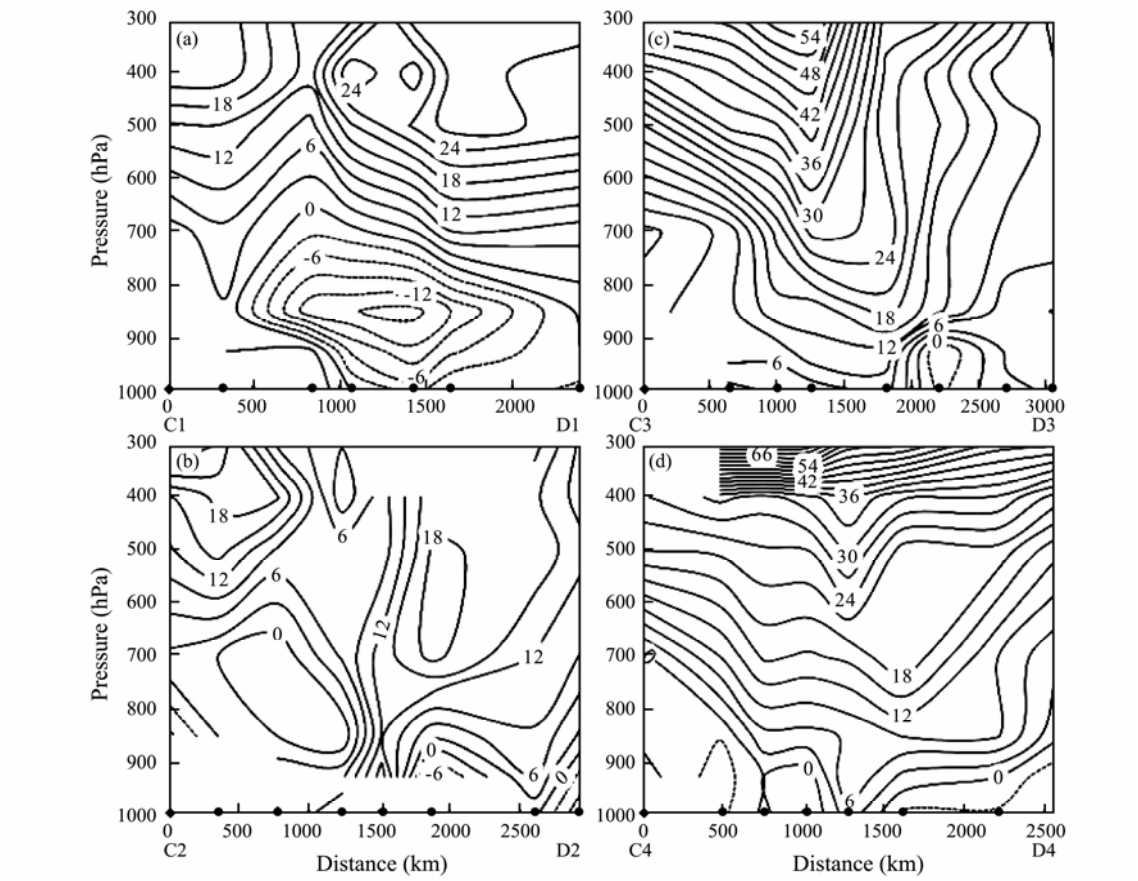

Fig.17 As in Fig.15, but for the zonal wind speed.

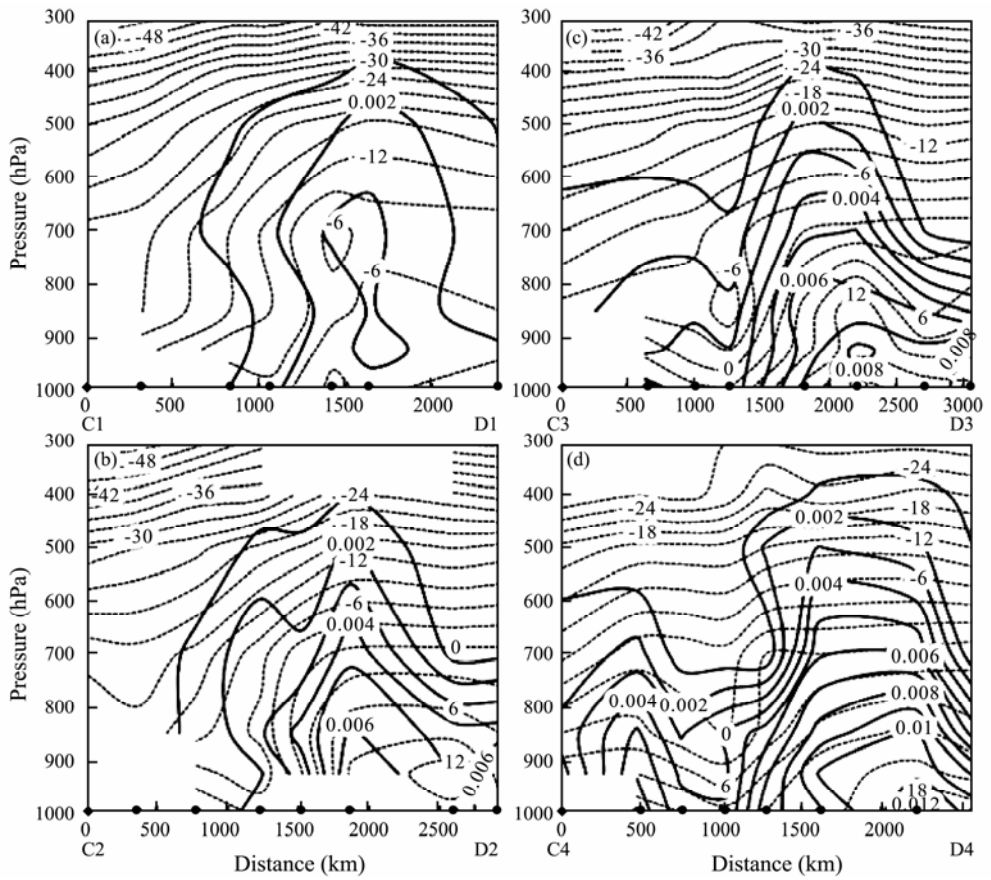

Fig.18 Vertical cross-section analyses along lines CiDi (I=1, 2, 3, 4) at 12 UTC 4 March 2007. Dashed lines represent the air temperature (℃), and solid lines represent specific humidity (kg kg^{-1}). The dots show the position of sounding stations.

5 Conclusions

We discussed the synoptic situation and mesoscale structure of an explosive extratropical cyclone that occurred over the Northwestern Pacific in March 2007. To summarize, a schematic diagram was created, as shown in Fig.19. Multiple factors may promote explosive cyclogenesis. The cyclone is located beneath the poleward side of the exit of 200 hPa jet, which is a strong divergent region. At the mid-level (500 hPa), the cyclone lies on the downstream side of a well-developed trough, where strong ascent motion frequently occurs. The cross-section analysis shows that the cyclone has a warm and moist core. A 'nose' structure appears when the cyclone moves offshore, and it might be caused by the heating effect of the Kuroshio Current; this is the first time that a 'nose' structure has been shown in observations. In addition, two low-level jet streams are identified on the western and eastern sides of the cold front. The western jet conveys cold and dry air at 800–900 hPa. The wind in the northern part is northeasterly, and the wind in the southern part is northwesterly. By contrast, the eastern jet carries warm and moist air into the cyclone system as it ascends northward from 900 hPa to 600–700 hPa. Moreover, the wind in the southern part is southerly, and the wind in the northern part is southwesterly.

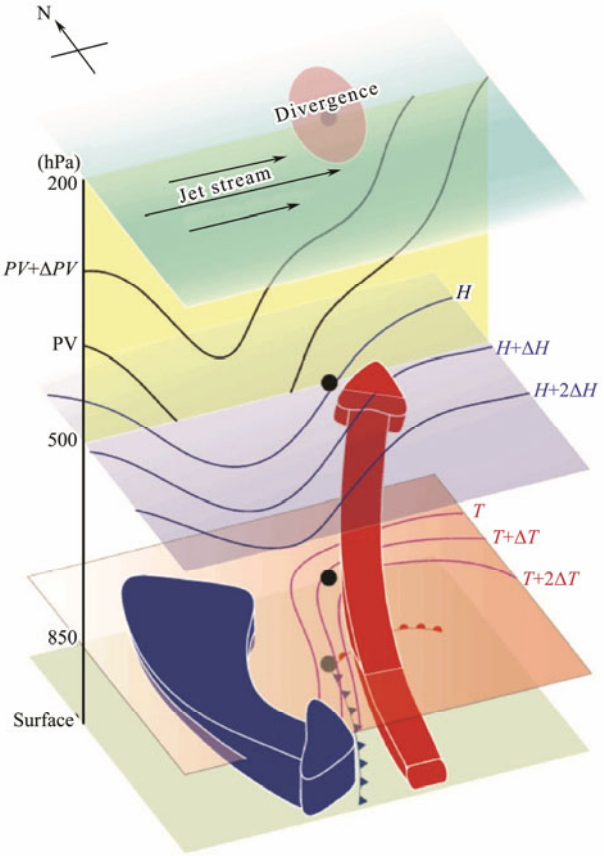

Fig.19 Schematic diagram of the cyclone at the developing stage. The blue arrow shows the west jet conveying cold and dry air, and the red arrow denotes the east jet carrying warm and moist air.

The 'nose' structure of the cold front and the low-level jet system are the two issues that we want to highlight in this study. Certain basic features of the explosive extratropical cyclone on a mesoscale were discussed by using observations from weather stations. However, additional studies, particularly a numerical simulation study, are needed to determine if the 'nose' structure commonly occurs when a cold front moves over a warm current. In addition, due to the spatially sparse distribution of weather stations in the ocean, the entire evolutionary processes of both the 'nose' structure and the jet system are not well documented. A high-resolution numerical simulation study on this subject needs to be conducted in the future.

Acknowledgements

This paper was financially supported by the National Natural Science Foundation of China (No. 41275049 and 41775042). All authors express their sincere thanks to Prof. Suping Zhang, Prof. Qi Wang, Prof. Shanhong Gao and Mr. Shuqin Zhang in Department of Marine Meteorology, Ocean University of China for their helpful discussions.

References

Anthes, R. A., Kuo, Y.-H., Benjamin, S. G., and Li, Y.-F., 1982. The evolution of the mesoscale environment of severe local storms: Preliminary modeling results. *Monthly Weather Review*, **110**: 1187-1213.

Bleck, R., 1974. Short-range prediction in isentropic coordinates with filtered and unfiltered numerical models. *Monthly Weather Review*, **102**: 813-829.

Bluestein, H. B., 1993. *Synoptic-Dynamic Meteorology in Midlatitudes. Volume II. Observations and Theory of Weather Systems*. Oxford University Press, New York, 606pp.

Bosart, L. F., and Lin, S. C., 1984. A diagnostic analysis of the Presidents' Day storm of February 1979. *Monthly Weather Review*, **112**: 2148-2177.

Böttger, H., Eckardt, M., and Katergiannakis, U., 1975. Forecasting extratropical storms with hurricane intensity using satellite information. *Journal of Applied Meteorology*, **14**: 1259-1265.

Gyakum, J. R., and Danielson, R. E., 2000. Analysis of meteorological precursors to ordinary and explosive cyclogenesis in the western North Pacific. *Monthly Weather Review*, **128**: 851-863.

Gyakum, J. R., Anderson, J. R., Grumm, R. H., and Gruner, E. L., 1989. North Pacific cold-season surface cyclone activity: 1975–1983. *Monthly Weather Review*, **117**: 1141-1155.

Hoskins, B. J., and Valdes, P. J., 1990. On the Existence of Storm-Tracks. *Journal of the Atmospheric Sciences*, **47**: 1854-1864.

Hoskins, B. J., McIntyre, M. E., and Robertson, A. W., 1985. On the use and significance of isentropic potential vorticity maps. *Quarterly Journal of the Royal Meteorological Society*, **111**: 877-946.

Iwao, K., Inatsu, M., and Kimoto, M., 2012. Recent changes in explosively developing extratropical cyclones over the winter northwestern Pacific. *Journal of Climate*, **25**: 7282-7296, DOI: 10.1175/JCLI-D-11-00373.1.

Lim, E.-P., and Simmonds, I., 2002. Explosive cyclone

development in the Southern Hemisphere and a comparison with Northern Hemisphere events. *Monthly Weather Review*, **130**: 2188-2209.

Reader, M. C., and Moore, G. W. K., 1995. Stratosphere and troposphere interactions associated with a case of explosive cyclogenesis in the Labrador Sea. *Tellus A*, **47**: 849-863.

Saha, S., Pan, H., Wu, X., Wang, J., Nadiga, S., Tripp, P., Kistler, R., Woollen, J., Behringer, D., Liu, H., Stokes, D., Grumbine, R., Gayno, G., Wang, J., Hou, Y., Chuang, H., Juang, H., Sela, J., Iredell, M., Treadon, R., Kleist, D., Van Delst, P., Keyser, D., Derber, J., Ek, M., Meng, J., Wei, H., Yang, R., Lord, S., Van Den Dool, H., Kumar, A., Wang, W., Long, C., Chelliah, M., Xue, Y., Huang, B., Schemm, J., Ebisuzaki, W., Lin, R., Xie, P., Chen, M., Zhou, S., Higgins, W., Zou, C., Liu, Q., Chen, Y., Han, Y., Cucurull, L., Reynolds, R., Rutledge, G., and Goldberg, M., 2010. The NCEP climate forecast system reanalysis. *Bulletin of the American Meteorological Society*, **91**: 1015-1057.

Sanders, F., and Gyakum, J. R., 1980. Synoptic-dynamic climatology of the 'bomb'. *Monthly Weather Review*, **108**: 1589-1606.

Sinclair, M. R., 1997. Objective identification of cyclones and their circulation intensity, and climatology. *Weather and Forecasting*, **12**: 595-612.

Uccellini, L. W., 1986. The possible influence of upstream upper-level baroclinic processes on the development of the QE II storm. *Monthly Weather Review*, **114**: 1019-1027.

Uccellini, L. W., and Kocin, P. J., 1987. The interaction of jet streak circulations during heavy snow events along the east coast of the United States. *Weather and Forecasting*, **2**: 289-308.

Uccellini, L. W., Keyser, D., Brill, K. F., and Wash, C. H., 1985. The Presidents' Day cyclone of 18–19 February 1979: Influence of upstream trough amplification and associated tropopause folding on rapid cyclogenesis. *Monthly Weather Review*, **113**: 962-988.

Uccellini, L. W., Kocin, P. J., Petersen, R. A., Wash, C. H., and Brill, K. F., 1984. The Presidents' Day cyclone of 18–19 February 1979: Synoptic overview and analysis of the subtropical jet streak influencing the pre-cyclogenetic period. *Monthly Weather Review*, **112**: 31-55.

Yoshida, A., and Asuma, Y., 2004. Structures and environment of explosively developing extratropical cyclones in the northwestern Pacific region. *Monthly Weather Review*, **132**: 1121-1142.

Zehnder, J. A., and Keyser, D., 1991. The influence of interior gradients of potential vorticity on rapid cyclogenesis. *Tellus* A, **43**: 198-212.

(Edited by Xie Jun)